Strain induced x-ray absorption linear dichroism in $La_{0.7}Sr_{0.3}MnO_3$ thin films

C. Aruta,[1,*] G. Ghiringhelli,[2] A. Tebano,[1] N. G. Boggio,[1] N. B. Brookes,[3] P. G. Medaglia,[1] and G. Balestrino[1]
[1]*CNR-INFM Coherentia and Dipartimento di Ingegneria Meccanica, Universita' di Roma Tor Vergata, Via del Politecnico 1, 00133 Roma, Italy*
[2]*CNR-INFM Coherentia and Dipartimento di Fisica, Politecnico di Milano, Piazza Leonardo da Vinci 32, 20133 Milano, Italy*
[3]*European Synchrotron Radiation Facility, Boîte Postale 220, 39043 Grenoble, France*
(Received 28 February 2006; revised manuscript received 16 May 2006; published 27 June 2006)

Strain induced anisotropy in the electronic properties of $La_{0.7}Sr_{0.3}MnO_3$ thin films was investigated by x-ray absorption spectroscopy at the Mn $2p$ and O $1s$ edges. Films on (100) $SrTiO_3$ and (100) $LaAlO_3$ substrates were grown by pulsed laser deposition with *in situ* reflection high energy electron diffraction diagnostic. At both absorption edges, clear features related to different anisotropic lattice strain effects as a function of the substrate were observed. On the average a negative (positive) linear dichroism was obtained for films grown under in-plane tensile (compressive) epitaxial strain conditions. Indeed, the structural macroscopic distortion induced by the substrate is responsible of the octahedra distortions with the resulting stabilization of x^2-y^2 ($3z^2$-r^2) orbitals. Enhanced linear dichroism at the Mn $2p$ edge in very thin films, only a few unit cells thick, is in agreement with a fully strained state which favors the formation of orbital ordered phase regions.

DOI: 10.1103/PhysRevB.73.235121 PACS number(s): 78.70.Dm, 68.60.Bs, 75.47.Lx

I. INTRODUCTION

For more than 50 years, mixed valence manganites $La_{1-x}A_xMnO_3$ (A=Ca, Sr, or Ba) have attracted the interest of researchers because of their noticeable physical properties. Namely, such compounds show a number of magnetic structures (various ferromagnetic and antiferromagnetic phases), metal-insulator electrical transitions, and various orbital and charge ordered states. Moreover, mixed valence manganites show novel phase separation phenomena at a nanometric scale,[1] which are thought to be a consequence of the interplay among several physical degrees of freedom (such as spin, charge, lattice, and orbital) simultaneously active in these materials.[2] Because of the complex interplay between the structural properties and the spin, charge, and orbital degrees of freedom, the effect of the structural distortions has been extensively investigated, in order to clarify its influence on the magnetotransport properties.[3–6] Two different mechanisms have been reported:[7]

(a) in the case of isotropic compressive strain the hopping probability between Mn^{3+} and Mn^{4+} ions increases as the Mn-Mn distance and the Mn–O–Mn bond angle decreases, thus enforcing the ferromagnetic ordering and the electron delocalization; and

(b) an additional effect originates in the case of biaxial strain ($\varepsilon_{xx}=\varepsilon_{yy}\neq\varepsilon_{zz}$), which can favor the stabilization of different $3d$ orbitals, depending on the octahedral distortion if in-plane compressive or tensile.

Biaxial strain states are obtained in epitaxial thin films grown on mismatched substrates. Under this respect, it has also been reported that, in manganite thin films, biaxial compressive or tensile strain can give rise to different orbital orderings, such as layer-type antiferromagnetic (A) and chain-type antiferromagnetic (C) states.[8] Therefore understanding the epitaxial strain effects on the electronic and orbital properties of thin films is of primary importance both for fundamental physics and possible applications. In this paper we have investigated $La_{0.7}Sr_{0.3}MnO_3$ (LSMO in the following) thin films grown on different substrates, under different strain conditions. The crystal structure of bulk LSMO is rhombohedral with a pseudocubic lattice parameter of $a=a_{rhomb}/\sqrt{2}$ $\sim$3.87 Å. In the case of thin films, grown on mismatched cubic substrates (100) oriented, a tetragonal distortion is induced, which varies the length of the perpendicular c lattice parameter. Several substrates can be used to induce different strain states in LSMO epitaxial thin films. We used (100)$SrTiO_3$ (STO), cubic with a_{sub}=3.905 Å, and (100) $LaAlO_3$ (LAO), rhombohedral with a pseudocubic lattice parameter of a_{sub}=3.786 Å, to induce tensile and compressive in-plane strain on LSMO films, respectively. In Ref. 9 the local structural distortion induced by substrate epitaxial strain around manganese atoms in LSMO films was investigated by x-ray absorption spectroscopy (XAS) at the Mn K edge. It was shown that biaxial strain induces a distortion of the MnO_6 octahedron, without changing the Mn-O-Mn angle. Furthermore, the linear dichroism (LD) in XAS can be measured by varying the polarization of the incoming synchrotron radiation. LD in XAS at the Mn $2p$ edge was proved to probe directly the orbital character of $3d$ states in orbital ordered manganites.[10] To study the strain induced anisotropy in the electronic properties of LSMO films, we have performed LD in XAS at Mn $2p$ edge and O $1s$ edge. The dominant photon-excited transitions at the Mn $2p$ edge are $2p\rightarrow 3d$, while at the O $1s$ edge are $1s\rightarrow 2p$, the latter being influenced by the orbital overlap with Mn $3d$. Because electronic and magnetic properties of manganites arise from the $3d$ electrons, which are exactly those affected by the structural distortions, the study of the LD spectra at the Mn $2p$ and O $1s$ edges is of primary importance for the comprehension of the biaxial strain effects on the electronic properties.

II. EXPERIMENT

High quality as-grown manganite films were grown at low oxygen pressures by pulsed laser deposition with *in situ* reflection high energy electron diffraction (RHEED) diagnos-

 ©2006 The American Physical Society

tic. The film deposition was carried out using an excimer laser charged with KrF (248 nm wavelength, pulse width 25 ns). The laser beam, with an energy per pulse of 1 mJ, was focused in a high vacuum chamber onto a target with an energy density per laser pulse of about 0.1 J/cm^2. The background atmosphere consisted of a mixture of O_2 with 10% ozone. The average background pressure in the chamber was fixed at 10^{-3} mbar and the substrate temperature at 650 °C. The mixture of molecular oxygen and ozone was injected through a narrow nozzle placed in close proximity to the plume. No postgrowth annealing treatments, either *in situ* or *ex situ*, were carried out on the films. Structural properties were measured by x-ray diffraction measurements (XRD) at Cu $K\alpha$ wavelength in the Bragg-Brentano configuration. Measurements were performed both in symmetrical and asymmetrical configurations to obtain the out-of-plane and in-plane lattice parameters, respectively. Electrical transport measurements were carried out by the standard four-probe technique as a function of the temperature. The resistivity values were deduced by using the Van der Pauw technique.[11] XAS measurements were performed at the ID08 beam line of the European Synchrotron Radiation Facility (ESRF). The beam line source is an AppleII undulator delivering ~100% polarized radiation. Measurements were carried out at the Mn 2*p* and O 1*s* edges varying the x-ray beam incidence angle and linear polarization direction in order to measure x-ray LD, from horizontal (*H*-polarization) to vertical (*V*-polarization) in the laboratory reference. For LD measurements the x-ray beam was set at 20° from the sample surface, so that the electric **E** vector was perpendicular to (*V*-polarization) or formed a 20° angle with (*H*-polarization) the film *c*-axis. The instrumental bandwidth of the monochromator (Dragon type) was set to 160 meV at the Mn 2*p* and to 115 meV at the O 1*s* edge. The pressure in the vacuum chamber was lower than 10^{-9} mbar during the measurements. We recorded XAS spectra by collecting the sample drain current.

III. RESULTS

A. Laser MBE growth process

The optimization of the physical properties of manganite films strongly depends on achieving the correct oxygen stoichiometry. The utilization of high oxygen pressure (about 0.1–1 mbar) during the growth severely restricts the full analytical capabilities of the conventional RHEED system for *in situ* control of growth. However, the film oxygen stoichiometry is strongly correlated with the laser fluence, and consequently with the plume oxidization. Therefore, in order to obtain the correct oxygen stoichiometry, together with the use of the RHEED diagnostic [Fig. 1(a)], we deposited the manganite films in the regime of low pressure (10^{-3} mbar) and low fluence, corresponding to deposition rates per pulse of about 10^{-3} unit cells/laser pulse, in which the film oxidation occurs primarily as a result of the plume-background interaction.[12] In this regime we obtained optimized manganite thin films with atomically flat surfaces, as confirmed by atomic force microscopy (AFM) studies [Fig. 1(b)] and without the need for any *in situ* or *ex situ* postgrowth annealing

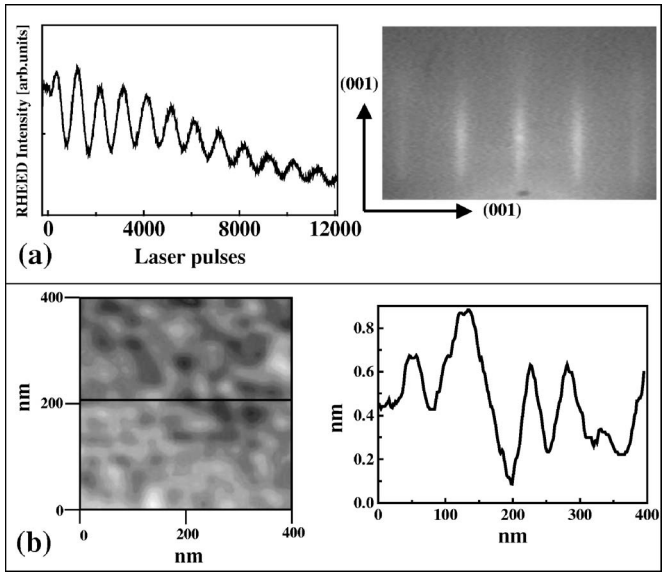

FIG. 1. (a) RHEED intensity oscillations during the deposition of a LSMO film (left); RHEED pattern at the end of the deposition process (right). (b) AFM surface topology image, 400×400 nm^2, for a 50 u.c. thick LSMO film on a LAO substrate (left); cross section along the marked line in the AFM image (right).

treatment. The utilization of the RHEED diagnostic *in situ*, monitoring the surface quality and the growth rate through the intensity oscillations of the RHEED specular spot, enabled very precise control of the layer by layer epitaxial growth and of the film thickness. Such precise control of the growth rate made the deposition of a very thin film with a thickness equal to 4 unit cells (u.c.) with an indetermination of about ±0.5 u.c. possible. Even in the case of thicker films, the surface roughness is well below 2 u.c., as demonstrated by the AFM image reported in Fig. 1(b) for a 50 u.c. thick LSMO film on (100) LAO substrate. In Fig. 1(a) we show typical intensity oscillations of the RHEED specular spot monitored during the initial stage of a LSMO film on STO deposition. The incident RHEED electron beam was parallel to the [100] direction of the substrate. From the RHEED intensity oscillations a deposition rate per pulse of about 10^{-3} u.c./laser pulse was calculated. The bidimensionality of the growth process was proved by the RHEED pattern which, at the end of the growth, showed typical 2D features [on the right of Fig. 1(a)].

B. Diffraction and transport measurements

Epitaxial LSMO films deposited on (100)STO and on (100)LAO substrates have opposite signs of the mismatch $m=(a_{sub}-a)/a_{sub}$: on (100)STO, films are under tensile strain with $m=+0.81\%$, while on (100)LAO, films are under compressive strain with $m=-2.2\%$. Strained layers start to relax upon reaching a critical thickness t_c, whose value depends both on the mismatch between film and substrate and film growth conditions. We found that LSMO films grown on STO substrates start to relax at a thickness above 100 u.c., while on LAO substrates the same phenomenon occurs at 40–50 u.c. This latter value is comparable with the typical t_c

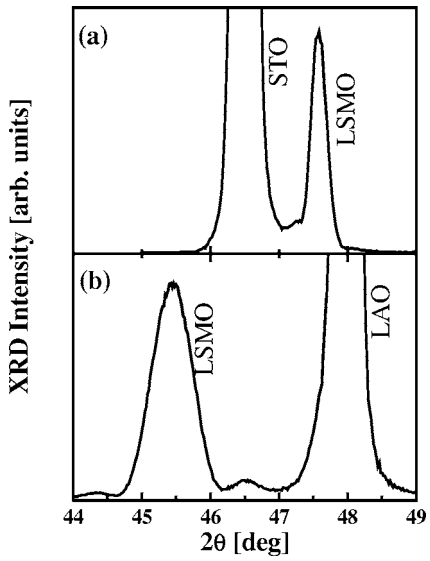

FIG. 2. X-ray diffraction measurements of the (002) reflections for the LSMO films: (a) 100 u.c. thick, grown on the STO substrate and (b) 30 u.c. thick, grown on the LAO substrate.

value reported in literature.[13] Asymmetric XRD diffraction measurements have demonstrated that our films grow epitaxially, cube on cube, relative to the substrate. In Fig. 2 we show the symmetric Θ-2Θ measurements around the (002) reflections for the fully strained LSMO films grown on STO (a) and on LAO (b) substrates. The out-of-plane c lattice parameter results to be 3.82 Å (for the film 100 u.c. thick on STO) and 3.99 Å (for the film 30 u.c. thick on LAO). The reciprocal space map around the asymmetric (103) reflections is reported in Fig. 3 for the two strained samples on STO and LAO substrates. In both cases, the diffraction spots, from the thin film and the corresponding substrate, show the same in-plane scattering vector Q_x, as expected for a perfect in-plane matching between film and substrate. However, the values of the out-of-plane scattering vector Q_z are quite different, in agreement with the elastic elongation (in the case of LAO) or compression (in the case of STO) of the out-of-plane lattice constant c. Relative to the perfect cubic unit cell ($c/a=1$), on the STO substrate the strained LSMO unit cell is compressed ($c/a=0.98$) and on the LAO substrate is elongated ($c/a=1.06$) out of the plane. For partially relaxed LSMO films on LAO the c/a ratio was found to decrease slightly relative to the 1.06 value. The in-plane strain is related to the perpendicular strain by the expression

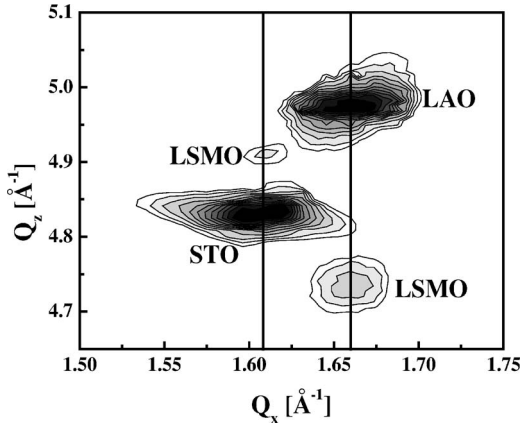

FIG. 3. Isointensity contour plot on a logarithmic scale of (103) reciprocal space map measured at Cu $K\alpha$ wavelength on fully strained LSMO thin films grown on STO and LAO substrates. The full vertical lines are connecting the (103) reflections of the films and the corresponding substrate. The range of the logarithmic scale is from 13 to 16 000.

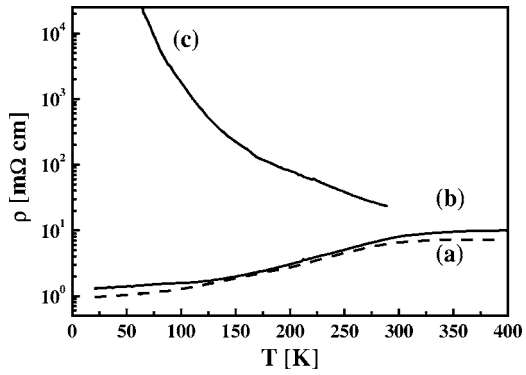

FIG. 4. Resistivity vs temperature behavior in logarithmic scale of LSMO films: (a) 100 u.c. on STO, (b) 100 u.c. on LAO, and (c) 30 u.c. on LAO.

$$\frac{\Delta c}{c} = -\frac{2\nu}{1-\nu}\frac{\Delta a}{a}.$$

In this formula ν represents the Poisson's ratio, and Δa and Δc are the lattice variations, in the plane and out of the plane, respectively, relative to the bulk values ($c=a$). The Poisson's ratio ν results to be about 0.40 for both compressive and tensile strain. The resistivity measurements as a function of the temperature of LSMO optimized samples, 100 u.c. thick, grown on STO and LAO substrates [Fig. 4 curves (a) and (b)], show metallic behavior with metal-insulator transition temperature (T_{MI}) of about 350 K, comparable with the values obtained for the single crystals.[14] LSMO films thinner than 30 u.c., deposited onto LAO, did not show any metal-insulator transition down to 20 K [Fig. 4(c)].

C. XAS measurements

1. Mn 2p edge

XAS measurements at the Mn $2p$ edges (mainly $2p \rightarrow 3d$ transitions) were recorded between 635 and 660 eV. The spin-orbit interaction of the Mn $2p$ core hole splits the spectrum into two broad multiplets, the L_3 ($2p_{3/2}$) edge at lower photon energy and the L_2 ($2p_{1/2}$) edge at higher photon energy. The peak shapes and chemical shifts are very sensitive to the $3d$ ground state configuration as well as the crystal-field interactions, and can be used to determine the $3d$ occupancy of the transition-metal ions.[15] In Fig. 5 we report XAS measurements in LSMO films on STO (fully strained, labeled LSMO-STO) and on LAO (partially relaxed, labeled LSMO-LAO1), both having a thickness of 100 u.c. and a

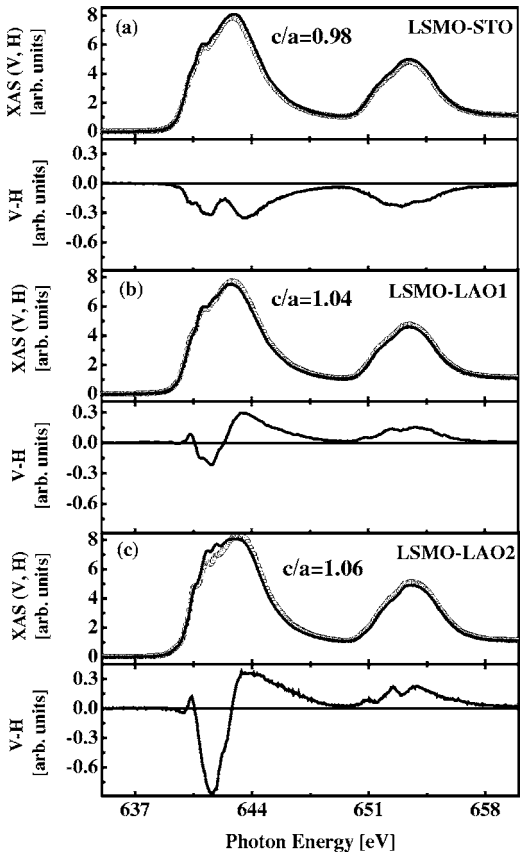

FIG. 5. XAS and LD at Mn $L_{2,3}$ edge of LSMO thin films 100 u.c. thick on STO (a), 100 u.c. thick on LAO (b), and 4 u.c. thick on LAO (c): XAS in *V*- and *H*-polarization (top); and linear dichroism $(V-H)$ (bottom).

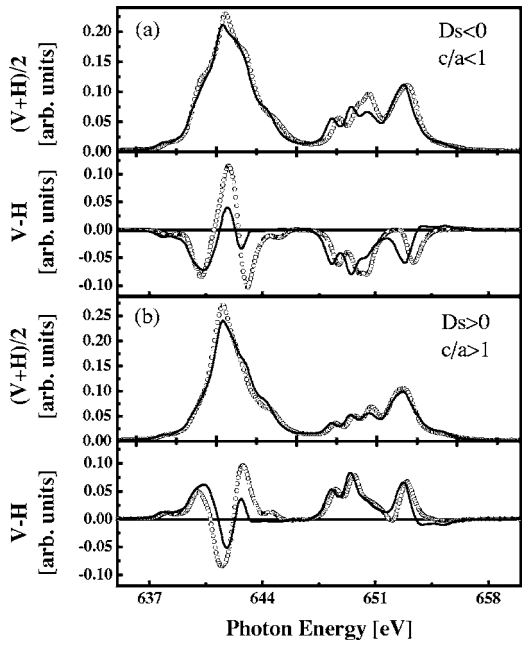

FIG. 6. Calculated XAS and LD in Mn^{3+} $L_{2,3}$ absorption with the value of $10Dq=1.1$ eV kept constant whereas the tetragonal distortion is changed: (a) $Ds=-0.025$ eV (line) and $=-0.186$ eV (line+circles); (b) $Ds=0.025$ eV (line) and $=0.186$ eV (line +circles). Top part: average between XAS in vertical and horizontal polarizations $(V+H)/2$; Bottom part: linear dichroism $(V-H)$.

third LSMO film on LAO (fully strained, labeled LSMO-LAO2) having a thickness of 4 u.c. (Table I). Samples have been measured in *H*- and *V*-polarization, which correspond roughly to investigate the out-of-plane and the in-plane directions, respectively. LD spectra have been obtained as the difference between the two measurements $(V-H)$. In order to extract the LD signal from XAS spectra recorded in two orthogonal linear polarizations, both spectra have to be superposed at low and high energy. Therefore a linear background was fitted to the preedge region of the L_3 edge and subtracted from the spectra, which are then normalized to the edge jump set to unity above the L_2 edge. Despite the relatively small LD effects, the results are univocal already from the raw data. The normalization procedure is safe and useful mainly to allow a more quantitative comparison of the LD in the different samples. Anisotropy effects induced by the substrate can be inferred from the LD spectra. Indeed, if we compare the two 100 u.c. thick LSMO films on the STO and on the LAO substrates, we can observe a different average sign for the LD spectra: namely a negative, on the average, LD spectrum was obtained in the case of tensile strain (LSMO-STO) while a positive, on the average, LD spectrum was obtained in the case of compressive strain (LSMO-LAO1). In the case of the LSMO-LAO2 film, the thickness is reduced well below the critical thickness t_c and the LD becomes more pronounced at about 641.5 eV, while maintaining the same qualitative features as for the thicker LSMO-LAO1 film. In Figure 6(b) we report the theoretical calculations performed with the Cowan's Hartree-Fock atomic code with point charge crystal field.[16] We used a single $3d^4$ configuration (Mn^{3+}), with spin-orbit interaction in the $3d$ and the $2p$ states, Slater integrals reduced to 70% of their atomic value. We found that our calculations were not very responsive to variations of the interatomic exchange interaction value, when it is varied between 0 and 30 meV, therefore we fixed it at 10 meV. A tetragonally distorted octahedral crystal field (D_{4h} symmetry) was used by resorting to the parameters *Ds* and *Dt*, which are related to the amount of tetragonal distortion by $\Delta e_g=4Ds+5Dt$ and $\Delta t_{2g}=3Ds-5Dt$, where Δe_g and Δt_{2g} are, respectively, the e_g and the t_{2g} levels splitting (see Fig. 7). We employed $10Dq=1.1$ eV for the cubic crystal field splitting, as optimized by comparing resonant inelastic x-ray scattering calculations and measurements on analogous samples.[17] In Fig. 6 we show two rather

TABLE I. Main crystallographic and transport properties for the three samples of Fig. 5.

Substrate	Thickness (u.c.)	c/a	T_{MI} (K)
LSMO-STO	100	0.98	350
LSMO-LAO1	100	1.04	350
LSMO-LAO2	4	1.06	

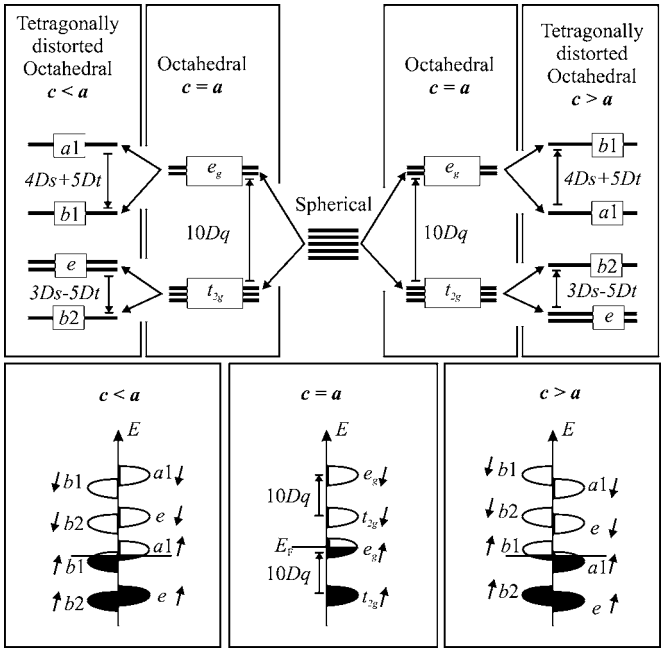

FIG. 7. Simplified scheme of the states energy. Top part: the crystal field splitting of the five Mn 3*d* atomic states in the cases of perfectly cubic ($c=a$, central panel), in-plane tensile ($c<a$, left panel), and in-plane compressive ($c>a$, right panel) strain. The intra-atomic exchange interaction splits the majority and minority states by an energy of the order of $10Dq$: we show here only one of the two spin states. The full atomic calculations done for Fig. 6 automatically accounts for the intra-atomic exchange interaction. In those calculations the interatomic exchange splitting was added (10 meV): this interaction further splits the atomic states (not shown in the scheme). Bottom part: a cartoon representation of the Mn-O hybridized states probed by O 1*s* XAS in the three different strain conditions. This scheme is based on the top part crystal field splitting of the Mn 3*d* states and on the assumption of a finite bandwidth of the O 2*p* states.

extreme cases of tetragonal distortion: a small value ($Ds=\pm 0.025$ eV, $Dt=\pm 0.0065$ eV, $\Delta e_g=140$ meV, $\Delta t_{2g}=40$ meV) and a relatively large one ($Ds=\pm 0.186$ eV, $Dt=\pm 0.030$ eV, $\Delta e_g=900$ meV, $\Delta t_{2g}=400$ meV). The sign of Ds and Dt indicates the type of distortion: positive values correspond to in-plane compressive deformations ($c>a$) and, conversely, negative values correspond to in-plane tensile deformations ($c<a$) of the octahedra. If we compare the calculations of Fig. 6 with the experimental results of Fig. 5, we observe that in the case of the STO substrate [Fig. 5(a)], the LD shape shows a general behavior similar to the one calculated for in-plane tensile strain [$c/a<1$, Fig. 6(b)]. In the case of the two LAO substrates [Figs. 5(b) and 5(c)], the general LD shapes are reversed relative to those of STO and are similar to the one calculated for in-plane compressive strain [$c/a>1$, Fig. 6(a)]. Moreover, the calculated LD spectra show that the amplitude of the linear dichroism effect is moderately influenced by the value of the crystal field splittings Δe_g and Δt_{2g}: in the simulated LD spectra the expected value is at least 5 times larger than what we have measured. This important finding will be discussed below, but we anticipate that we have explored a variety of parameters for the calculations such as a value for $10Dq$ of the order of 2 eV and higher values of the temperature, without obtaining a consistent reduction of the calculated LD effect.

2. O 1*s* edge

XAS at the O 1*s* edge (mainly $1s\rightarrow 2p$ transitions) were recorded between 522 and 558 eV. As demonstrated by Grioni *et al.*[18] the O 1*s* spectra map mainly the unoccupied electronic structure at the metal sites, since the O 2*p* states are hybridized with the metal states, forming empty bands of predominantly metal character above the Fermi level, but reachable in a dipole allowed $1s\rightarrow 2p$ transition taking place at an oxygen site. This property allows us to use the O 1*s* edge LD to determine the local symmetry of the Mn empty states. In Fig. 8 the XAS spectra for the 100 u.c. thick LSMO films grown on STO and LAO substrates are reported. We do not report oxygen data on thinner films due to the contribution from the oxygen in the substrate. Abbate *et al.*[19] demonstrated the heavily mixed metal-ligand character of the LSMO compound and they assigned the main peak at about 530 eV to the orbital overlap with the Mn 3*d*, the peak at about 536 eV to the bands with La 5*d*/Sr 4*d* character, and finally the peak at about 545 eV to the bands with Mn 4 *sp* character. In Fig. 8 we show the spectra measured on the two films together with the spectra of the STO and LAO substrates, including their LD: very likely the contribution coming from the substrates is negligible in the whole energy range, but it has to be noted that below 530 eV the substrates give zero contribution, so that what it is observed on the first peak is genuinely coming from the LSMO films. We have carefully checked that no derivative effects, possibly related to spurious energy shifts during the measurements, were present in our data. After normalization of the spectra above and below the oxygen absorption edge, the average intensity is comparable for the two substrates, in agreement with a similar oxygenation of the samples. However, the main features of LD spectra are reversed relative to each other in the two LSMO films. In particular the 528–530 eV interval shows a perfect reversal of the LD spectrum [Fig. 8(c)]. As already shown by Wu *et al.*[20] the oxygen *K* edge LD is a direct probe of the Mn 3*d* orbital close to the Fermi level. In the case of LAO [Fig. 8(b)] the compressive strain raises the energy of the $b1$ (x^2-y^2) state above the Fermi level, giving a positive LD at the main peak at 530 eV and a negative LD at the 529 eV onset. The opposite happens for the STO substrate [Fig. 8(a)]: the negative peak at about 530 eV is of $a1$ symmetry, the positive peak at 529 eV is of $b1$ symmetry. In Fig. 7 we show an oversimplified scheme of the states energy. It is not possible to directly read the O 2*p* edge XAS spectra as a measurement of the partial density of states, due to the different hybridization of the states and to the radiative transition cross-section issues. Nevertheless we can use the LD to deduce that the 533 eV peak has possibly a t_{2g} minority character and that the e_g minority states are distributed between 533 and 535 eV. In fact the LD curves show a negative-positive (positive-negative) behavior in such energy range for the LAO (STO) substrate in analogy to the 529 to 530 eV region, whereas at 533 eV the two LD have the same sign.

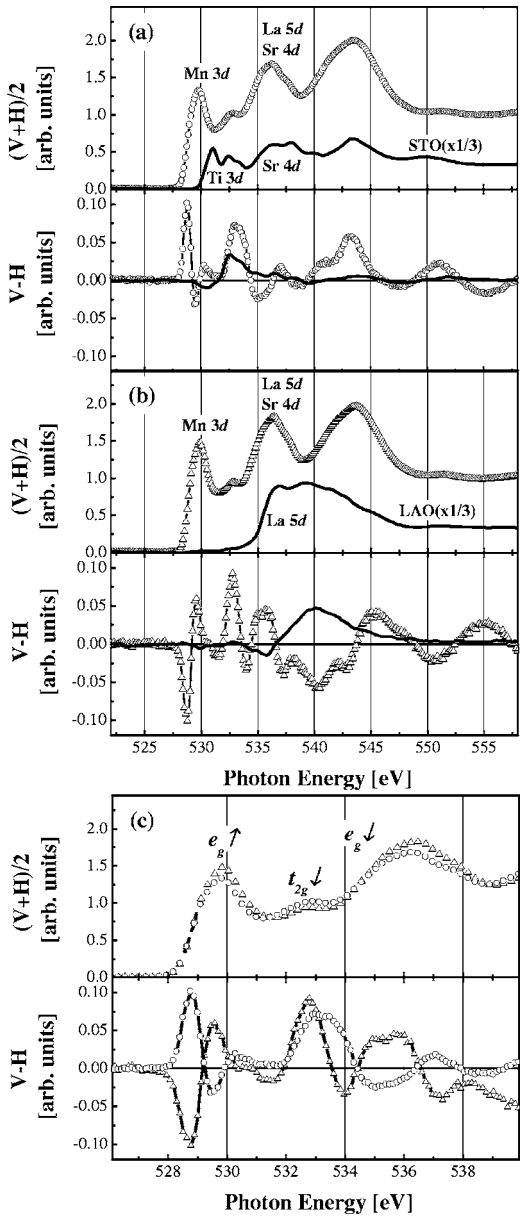

FIG. 8. O 1*s* edge XAS and LD spectra for LSMO thin films (lines+symbols) and the corresponding substrates (lines): STO (a) and LAO (b). (c) Comparison between the spectra of films on STO (line+circles) and on LAO (line+triangles) highlighted between 526 and 540 eV.

This type of rough analysis seems to indicate that the cubic crystal field splitting can be of the order of 1 eV, and that the tetragonal distortion crystal field is much smaller than the intrinsic width of the Mn states projected onto the O 2*p* band.

IV. DISCUSSION

The LD spectrum at Mn $L_{2,3}$ XAS [(b) in Fig. 5] for the 100 u.c. thick film grown on a LAO substrate (subjected to compressive epitaxial strain) indicates a preferential occupation of the out-of-plane $3z^2$-r^2 orbitals. The stabilization of the $3z^2$-r^2 orbitals is a consequence of the tetragonal distortion, induced by the epitaxial strain, which increases the Mn–O bond length along the out-of-plane direction. On the contrary, the LD spectrum in Fig. 5(a), in the case of the film subjected to tensile epitaxial strain (100 u.c. thick film grown on a STO substrate), gives evidence of a preferential occupation of the in-plane x^2-y^2 orbitals as a consequence of the decrease of the in-plane Mn–O bond lengths. Experimental results are in reasonable agreement with theoretical calculations, shown in Fig. 6. Such calculations were based exclusively on the Mn^{3+} contribution. Although the LD behavior should not be affected by the 3*d* orbitals of Mn^{4+}, nevertheless the absorption contribution of the Mn^{4+} ions could give rise to a decrease of the LD relative intensity. Results from the LD spectra at the O 1*s* edge (Fig. 8) agree with those obtained for the Mn 2*p* edge. Namely, we found that the LD signal at the main peak at 530 eV, mostly influenced by the Mn 3*d* atoms, is negative in the case of STO and positive in the case of LAO. Such a finding is in agreement with an x^2-y^2 and $3z^2$-r^2 stabilization of 3*d* Mn orbitals for films grown on STO and on LAO substrates, respectively. Moreover, Fig. 5 shows that the intensity of LD at the Mn 2*p* edge is comparable for films having the same thickness (LSMO-STO and LSMO-LAO1), while it is larger for the thinner film (LSMO-LAO2). Even though the calculations of Fig. 6 show an increase of the LD spectra with the *Ds* value, the tetragonal crystal field effect alone cannot explain the large LD variation in the experimental data between the 100 and 4 u.c. thick films. In the case of 100 u.c. thick films the c/a value is found to be 0.98 and 1.04 for the LSMO-STO and LSMO-LAO1 sample, respectively, as reported in Table I. This means that XRD measurements show that LSMO-STO is fully strained whereas LSMO-LAO1 is partially relaxed because it exceeds the critical thickness. However, by the bulk sensitive XRD measurements we cannot rule out the existence, even in the case of the film on STO, of a partial relaxation in the topmost layers, which are mostly probed by the surface sensitive XAS technique. On the contrary the 4 u.c. thick film LSMO-LAO2, whose thickness is well below the critical value of about 40–50 u.c., can be considered fully strained with a c/a ratio equal to 1.06. The phase diagram first proposed by Konishi and coworkers,[8] and then explained theoretically by Fang and co-workers,[3] accounts well for the experimental behavior of the LD signal in our epitaxially strained films. According to the above phase diagram the epitaxial strain for the 100 u.c. thick films on STO ($c/a=0.98$) and on LAO ($c/a=1.04$) is not large enough to force an antiferromagnetic orbital ordered phase of the A- and C-type, respectively. On the contrary, in the case of the completely strained LSMO-LAO2 film, the c/a ratio of 1.06 is such to put the representative point of the film in the C antiferromagnetic orbital ordered region (Fig. 3 in Ref. 8), even if very close to the transition line to the F metallic-ferromagnetic orbital disordered phase. However, even in the case of the 100 u.c. thick film on LAO, because of its partial relaxation, the presence of strained layers can be responsible for the LD measured in such a thicker film. This analysis is confirmed by the electrical transport measurements of Fig. 4. Such a figure shows a "metallic" behavior for the 100 u.c.

thick films on STO and on LAO, while the resistivity behavior is insulating for the fully strained film on LAO ($c/a = 1.06$). Such findings are in agreement with the scenario proposed by Souza-Neto and co-workers,[9] in which the main strain effect is to induce a variation of the c/a ratio without affecting the Mn–O–Mn bond angles. Indeed, both the c/a representative points of the 100 u.c. thick films on LAO and on STO substrates are in the F metallic-ferromagnetic region of the phase diagram reported in Fig. 3 of Ref. 8. In addition, the comparable amplitude of the LD spectra [Figs. 5(a) and 5(b)] indicates a comparable percentage of occupation of $3z^2$-r^2 or x^2-y^2 orbitals in the case of the film on LAO or on STO, respectively. A comparable percentage of distorted octahedra can be thus envisaged and it can explain the similar transport measurements reported in Fig. 4 [curves (a) and (b)], with almost the same T_{MI} transition temperature for both the 100 u.c. thick films. The interpretation of the LD spectra of the epitaxially strained manganite thin films outlined above finds strong support in recent XAS linear dichroism measurements carried out on various antiferromagnetic orbital ordered manganites of different compositions, including $La_{1-x}Sr_{1+x}MnO_4$ layered manganites.[10,20] For instance, a remarkable agreement can be noticed between the experimental LD spectrum of the $LaSrMnO_4$ layered manganite (Fig. 1 of Ref. 10), which exhibits a C-type antiferromagnetic $3z^2$-r^2 ordering, and the experimental spectrum of the LSMO film fully strained on a LAO substrate [Fig. 5(c)]. However, while the shape of the LD spectrum is remarkably similar, a difference can be noticed in the amplitude of the LD signal, which is larger in the case of layered manganites relative to the fully strained film on LAO. The reduction of the LD signal can be tentatively explained by the occurrence of nanometric phase separation between the C-type antiferromagnetic insulating phase and the F-type ferromagnetic metallic phase. Phase separation on a nanometric scale has been experimentally proved by scanning tunnel spectroscopy in the case of both $La_{0.7}Sr_{0.3}MnO_3$ and $La_{0.7}Ca_{0.3}MnO_3$ films[21] and associated with a nonuniform strain in the island 3D growth mode occurring in mismatched films.[22] In the case of the fully strained film on LAO, phase separation phenomena can be favored by the proximity to the F-phase stability region. Mixing of C- and F-phases would lead to a decrease of the intensity of the LD signal in comparison with fully ordered systems.

V. CONCLUSION

We have performed LD in XAS measurements on LSMO thin films grown by laser MBE on STO and LAO substrates in a 2D layer-by-layer mode. The different mismatch between film and substrate gives rise to different biaxial strain. Epitaxial strain was measured by XRD measurements. Partial relaxation of epitaxial strain was found in the case of the LAO substrates for film thickness above 40–50 u.c., while films on STO substrates resulted strained up to 100 u.c. The in-plane compressive or tensile strain induced a macroscopic crystallographic distortion, which in turn affected the octahedra distortion. The in-plane compression or elongation of the Mn–O bond lengths resulted in the stabilization of the $3z^2$-r^2 or the x^2-y^2 orbitals, giving rise to a different XAS linear dichroism. Theoretical simulations were in satisfactory agreement with experimental LD results. In the case of thinner, fully strained films on LAO, the LD signal showed a somewhat different behavior which compares very well with those reported for fully orbital ordered C-type manganites. Such a finding is in agreement with the c/a versus x (in $La_{1-x}Sr_xMnO_3$) phase diagram proposed in Ref. 8. The relatively lower intensity of the dichroic signal in the case of strained films was tentatively explained as a phase separation phenomenon enhanced by the proximity to the C antiferromagnetic–F ferromagnetic transition.

ACKNOWLEDGMENTS

The authors thank Vittorio Cataudella and Francesco Borgatti for valuable discussions, and Claudia Dallera and Riccardo Gusmeroli for making the graphical user interface of the Cowan code used for the simulations of Fig. 6 available.

*Electronic address: carmela.aruta@uniroma2.it

[1] Adriana Moreo, Seiji Yunoki, and Elbio Dagotto, Science **283**, 2034 (1999).
[2] E. Dagotto, Science **309**, 257 (2005).
[3] Z. Fang, I. V. Solovyev, and K. Terakura, Phys. Rev. Lett. **84**, 3169 (2000).
[4] M. Bibes, S. Valencia, Ll. Balcells, B. Martinez, J. Fontcuberta, M. Wojcik, S. Nadolski, and E. Jedryka, Phys. Rev. B **66**, 134416 (2002).
[5] J. Klein, J. B. Philipp, G. Carbone, A. Vigliante, L. Alff, and R. Gross, Phys. Rev. B **66**, 052414 (2002).
[6] J. Klein, J. B. Philipp, D. Reisinger, M. Opel, A. Marx, A. Erb, L. Alff, and R. Gross, J. Appl. Phys. **93**, 7373 (2003).
[7] A. J. Millis, T. Darling, and A. Migliori, J. Appl. Phys. **83**, 1588 (1998).
[8] Y. Konishi, Z. Fang, M. Izumi, T. Manako, M. Kasai, H. Kuwahara, M. Kawasaki, K. Terakura, and Y. Tokura, J. Phys. Soc. Jpn. **68**, 3790 (1999).
[9] N. M. Souza-Neto, A. Y. Ramos, H. C. N. Tolentino, E. Favre-Nicolin, and L. Ranno, Phys. Rev. B **70**, 174451 (2004), and references therein.
[10] D. J. Huang, W. B. Wu, G. Y. Guo, H.-J. Lin, T. Y. Hou, C. F. Chang, C. T. Chen, A. Fujimori, T. Kimura, H. B. Huang, A. Tanaka, and T. Jo, Phys. Rev. Lett. **92**, 087202 (2004).
[11] L. J. van der Pauw, Philips Tech. Rev. **20**, 220 (1958).
[12] A. Tebano, G. Balestrino, N. G. Boggio, C. Aruta, B. Davidson, and P. G. Medaglia, Eur. Phys. J. B (to be published).
[13] A. M. Haghiri-Gosnet, J. Wolfman, B. Mercey, Ch. Simon, P. Lecoeur, M. Korzenski, M. Hervieu, R. Desfeux, and G. Baldinozzi, J. Appl. Phys. **88**, 4257 (2000); A. Yu. Petrov, C. Aruta, S. Mercone, C. Adamo, I. Alessandri, and L. Maritato, Eur. Phys. J. B **40**, 11 (2004).

[14] A. Urushibara, Y. Moritomo, T. Arima, A. Asamitsu, G. Kido, and Y. Tokura, Phys. Rev. B **51**, 14103 (1995).
[15] F. M. F. de Groot, J. C. Fuggle, B. T. Thole, and G. A. Sawatzky, Phys. Rev. B **41**, 928 (1990).
[16] R. D. Cowan, *The Theory of Atomic Structure and Spectra* (University of California Press, Berkeley, 1981).
[17] G. Ghiringhelli *et al.* (unpublished).
[18] M. Grioni, M. T. Czyzyk, F. M. F. de Groot, J. C. Fuggle, and B. E. Watts, Phys. Rev. B **39**, 4886 (1990).
[19] M. Abbate, F. M. F. de Groot, J. C. Fuggle, A. Fujimori, O. Strebel, F. Lopez, M. Domke, G. Kaindl, G. A. Sawatzky, M. Takano, Y. Takeda, H. Eisaki, and S. Uchida, Phys. Rev. B **46**, 4511 (1992).
[20] W. B. Wu, D. J. Huang, G. Y. Guo, H.-J Lin, T. Y. Hou, C. F. Chang, C. T. Chen, A. Fujimori, T. Kimura, H. B. Huang, A. Tanaka, and T. Jo, J. Electron Spectrosc. Relat. Phenom. **137**, 641 (2004).
[21] T. Becker, C. Streng, Y. Luo, V. Moshnyaga, B. Damaschke, N. Shannon, and K. Samwer, Phys. Rev. Lett. **89**, 237203 (2002).
[22] Amlan Biswas, M. Rajeswari, R. C. Srivastava, T. Venkatesan, R. L. Greene, Q. Lu, A. L. de Lozanne, and A. J. Millis, Phys. Rev. B **63**, 184424 (2001).